Theoretical Analysis of 3-D Channel Spatial Correlation and Capacity

Yawei Yu, Jianhua Zhang, Peter J. Smith, and Pawel A. Dmochowski

Abstract—An approximate closed-form expression for 3-D channel spatial correlation (SC) is derived, given cross-polarized rectangular arrays and standards-based antenna radiation patterns. Furthermore, we evaluate the impact of 3-D SC on system performance and derive the capacity relationship between 2-D and 3-D channels. As expected, the 3-D channel is characterized by lower SC and higher channel capacity than its 2-D counterpart by taking the advantage of the additional degrees of freedom in the elevation domain, where the 3-D antenna arrays and the 3-D channel propagation are considered.

Index Terms—3D SC, channel capacity.

I. INTRODUCTION

TO MEET the high capacity demand in 5G communication [1], 3D MIMO, which fully utilizes the elevation domain to enable flexible strategies [2], has been investigated. Preliminary results on 3D channel modeling has been reported [3], recent measurements demonstrate a large capacity gap between 2D and 3D channel models [4]. As analyzed in [5], much is attributed to the reduction in the antenna spatial correlation (SC) with the increase in vertical antenna spacing (VAS) and elevation angle spread (EAS). Under different angle spreads and antenna spacings, closed-form expressions of 3D SC for various antenna arrays were investigated in [6]. However, [6] did not consider practical antenna radiation patterns due to the lack of standardized 3D models even though system performance is closely related to antenna radiation efficiencies [7]. Based on the Fourier coefficients of antenna radiation patterns, a general closed-form expression for 3D SC for a uniform linear antenna array was proposed in [8]. Based this prior work, we make the following contributions:

- Given a cross-polarized uniform rectangular array (URA) and standards based antenna radiation patterns [9], we derive and evaluate an approximate closed-form expression for 3D SC.
- Numerical simulation results demonstrate that when VAS = 0.5λ, 3D SC will be lowered to 0.60, 0.52, 0.35 for EAS = 30°, 60° and 90°, respectively.
- We derive bounds for 3D channel capacity, which show a clear relationship between 2D and 3D channel capacity. A large channel capacity increase (>38% at EAS=10°)
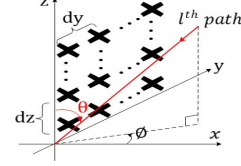
Fig. 1.   URA with cross-polarized antenna pairs.

from 2D to 3D channels has been observed, and this gap is further enhanced with larger EAS.

- We conclude that the 3D channel will achieve lower SC and higher channel capacity than its 2D counterpart due to the additional freedom in the elevation domain, which highlights the importance of 3D channel utilization.

Notation: $U(a,b)$, $VM(\mu_0,\kappa)$, $\mathcal{CN}(\mu_1,\sigma^2)$, $J_0(\cdot)/I_0(\cdot)$, $\odot$ denote the uniform distribution within (a,b), Von-Mises distribution with mean value μ_0 and dispersion factor κ, complex Gaussian distribution with mean value μ_1 and standard derivation σ, the zeroth order modified Bessel function of the first/second kind, the Hadamard product, respectively.

II. CLOSED FORM EXPRESSION FOR 3D SC

Given the 3D channel model [9] and the elevation angle θ and azimuth angle ϕ are independent, the 3D SC between element m and m' of the URA in Fig. 1 is given by [5]

$$R_{mm'}^{3D} = \begin{cases} \dfrac{\mathbb{E}\{A_V(\theta)A_H(\phi)e^{-j2\pi r^T(d_m-d_{m'})}\}}{\mathbb{E}\{A_V(\theta)\}\mathbb{E}\{A_H(\phi)\}} & \text{for } \xi_m=\xi_{m'}, \\ 0 & \text{for } |\xi_m-\xi_{m'}|=\pi/2, \end{cases} \quad (1)$$

where

- $A_V(\theta)$ and $A_H(\phi)$ denote the antenna radiation patterns in the elevation and azimuth domain, where

$$A_V(\theta)\text{B} = -\min\left[12\left(\frac{\theta-90^o}{\theta_{3\text{dB}}}\right)^2, SLA_v\right],$$
$$\theta_{3\text{dB}} = 65^o, \quad SLA_v = 30 \text{ dB}, \quad (2)$$
$$A_H(\phi) \text{ dB} = -\min\left[12\left(\frac{\phi}{\phi_{3\text{dB}}}\right)^2, A_m\right],$$
$$\phi_{3\text{dB}} = 65^o, \quad A_m = 30 \text{ dB}. \quad (3)$$

- r denotes the spherical unit vector of the transmitted (or received) path

$$r = [\sin(\theta)\cos(\phi), \sin(\theta)\sin(\phi), \cos(\theta)]^T. \quad (4)$$

- d_m and $d_{m'}$ denote the location vectors of element m and m', respectively, given by

$$d_m = (dx_m, dy_m, dz_m)^T, \quad d_{m'} = (dx_{m'}, dy_{m'}, dz_{m'})^T. \quad (5)$$

- ξ_m and $\xi_{m'}$ denote the polarization slant angles of the antenna m and m', respectively.

Since $R_{mm'}^{3D}$ is zero for cross-polarized antennas with $|\xi_m - \xi_{m'}| = \frac{\pi}{2}$ [5], we focus on $R_{m,m'}^{3D}$ for co-polarized antennas where $\xi_m = \xi_{m'}$ and derive its closed-form expression.
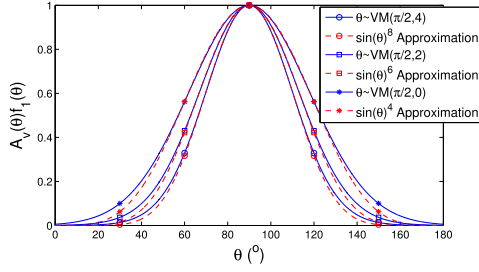
Fig. 2. Approximation accuracy of $\sin(\theta)^{2L}$.

(a) $R^{3D}_{mm'}(0, dy, 0)$ with d_y

(b) $R^{3D}_{mm'}(0, 0, dz)$ with d_z

Fig. 3. Variation of $R^{3D}_{mm'}(d_x, d_y, d_z)$ with d_y and d_z.

Lemma 1: Assuming $\phi \sim U(-\pi, \pi)$ and $\theta \sim VM(\frac{\pi}{2}, \kappa)$ [8], the approximate closed-form expression for $R^{3D}_{mm'}$ is given in (6), at the bottom of this page, where

- d_{xy} is distance between elements m, m' in the $x - y$ plane

$$d_{xy} = \sqrt{d_x^2 + d_y^2}, \qquad (7)$$

  where d_x and d_y denote the spacing between elements m and m' along x axis and y axis, respectively. Here we ignore the index m and m' for simplicity.

- Δ is related to d_x and d_y by $\Delta = \tan^{-1}(d_y/d_x)$.
- $\{a_n, n = 0, 1, 2, \ldots, N\}$ are the Fourier series coefficients of $A_H(x)$ given by

$$a_0 = \frac{1}{2\pi} \int_{-\pi}^{\pi} A_H(x)dx,$$
$$a_n = \frac{1}{\pi} \int_{-\pi}^{\pi} A_H(x) \cos(nx)dx. \qquad (8)$$

- A series expansion we use where $e^{-j2\pi d_z \cos\theta}$

$$= J_0(-2\pi d_z) + 2\sum_{r=1}^{R} j^r J_r(-2\pi d_z)\cos(r\theta). \qquad (9)$$

- N_{1r}, N_{2r} are given by

$$N_{1r} = (n - l)/2, \quad N_{2r} = (n + l)/2. \qquad (10)$$

- The probability density function, $f(\theta)$, for a Von-Mises distribution is given by

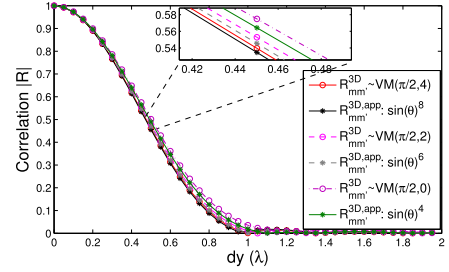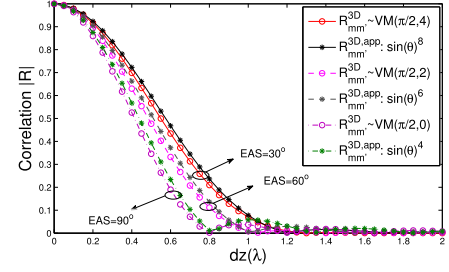$$f(\theta) = e^{\kappa \sin\theta}/(2\pi I_0(\kappa)) = c_\kappa f_1(\theta), \qquad (11)$$

  where $f_1(\theta) = e^{\kappa \sin\theta}/e^\kappa$ and $c_\kappa = e^\kappa/(2\pi I_0(\kappa))$.

- k_l ($l = 0, 1, 2, \ldots$) denote the expansion coefficients of $\sin(\theta)^{2L}$ in (22) and are given by

$$k_0 = \frac{1}{2^{2L}}\binom{2L}{L}, \quad k_l = \frac{1}{2^{2L}}(-1)^l 2\binom{2L}{L-1} \text{ for } l > 0. \quad (12)$$

Proof: See Appendix IV-A.

Note that, $A_V(\theta) f_1(\theta) \approx \sin(\theta)^{2L}$ is the only approximation used in deriving (6) and suitable for other elevation angle distributions such as Laplacian, Wrapped Guassian, etc. For the narrower Von-Mises distributions (larger κ), a larger value of L is needed. For example, when $\kappa = 4, 2, 0$ (EAS values are $30^o, 60^o, 90°$), we approximate the term $A_V(\theta) f_1(\theta)$ by

$\sin(\theta)^8$, $\sin(\theta)^6$ and $\sin(\theta)^4$, respectively, and the approximation accuracy is validated in Fig. 2.

Fig. 3 shows the variation of $R^{3D}_{m,m'}$ with d_y and d_z under different EASs (different κ). As $a_n \to 0$ rapidly as n increases, using only a few terms (say $N = 5$) gives a high accuracy. Similarly, a small number of the expansion terms in (9) is used (say $R = 4$). The larger antenna spacing in the y or z axis greatly reduces the SC. When d_y or d_z reaches 0.5λ, the SC is lowered to 0.5 approximately. Larger EAS will lower the SC in Fig. 3(b) while $R^{3D}_{mm'}$ for different EASs in Fig. 3(a) shows minor differences when $d_z = 0$. For the above cases, the approximate 3D SC in (6), $R^{3D,app}_{mm'}$, fits well with the true value $R^{3D}_{mm'}$. Thus, the derivation of (6) provides a general method to calculate the closed-form expression for 3D SC with high approximation accuracy.

III. CHANNEL CAPACITY

The 3D SC is given for a cluster-based channel model (CBCM), where the capacity gap between 2D and 3D channel models is difficult to derive. Results in [10] show a close similarity between eigenvalues of the CBCM and Kronecker channel model. This implies that we could apply the calculated SC to a Kronecker channel model in the ergodic capacity analysis to obtain the capacity relationship between 2D and 3D channels. Assuming a simple Rayleigh fading channel

$$\mathbf{H} = \mathbf{R}_{Rx}^{1/2}\mathbf{G}\mathbf{R}_{Tx}^{1/2}, \qquad (13)$$

where $\mathbf{G} \in \mathcal{C}^{Q \times M}$ has $\mathcal{CN}(0, 1)$ entries and M/Q denote the Tx/Rx antenna number. The capacity is computed as [11]

$$C = \mathbb{E}\left\{\log_2 \det\left(\mathbf{I} + \frac{\text{SNR}}{\beta M}\mathbf{H}^H\mathbf{H}\right)\right\}, \qquad (14)$$

$$R^{3D}_{m,m'} \approx R^{3D,app}_{mm'} = \frac{1}{\pi a_0 k_0} \sum_{n=0}^{N} a_n(-j)^n \cos(n\Delta) \left\{ \sum_{l=0}^{L} k_l \pi \left[J_0(-2\pi d_z) J_{\frac{n}{2}-l}(\pi d_{xy}) J_{\frac{n}{2}+l}(\pi d_{xy}) + \sum_{r=1}^{R} j^r \right. \right.$$
$$\left. \left. \times J_r(-2\pi d_z) \left(\cos(N_{1r}\pi) J_{\frac{n}{2}-N_{1r}}(\pi d_{xy}) J_{\frac{n}{2}+N_{1r}}(\pi d_{xy}) + \cos(N_{2r}\pi) J_{\frac{n}{2}-N_{2r}}(\pi d_{xy}) J_{\frac{n}{2}+N_{2r}}(\pi d_{xy}) \right) \right] \right\}, \quad (6)$$
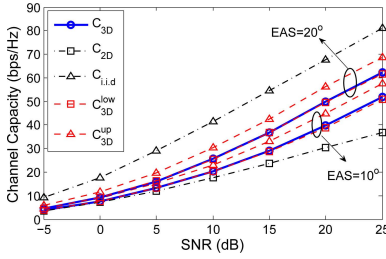
Fig. 4.   Channel capacity: loose and tight bounds for C_{3D}.

where β is the normalization factor, thus $\mathbb{E}\left\{\frac{1}{\beta}\|\mathbf{H}\|_F^2\right\} = MQ$.

Lemma 2: 2D capacity, C_{2D}, and the bounding 3D capacity, C_{3D}^B, are given below:

$$C_{2D} = \mathbb{E}\left\{\log_2 \det\left(\mathbf{I} + \frac{\text{SNR}}{\beta M}\mathbf{G}^H \mathbf{R}_{Rx}^{2D}\mathbf{G}\mathbf{R}_{Tx}^{2D}\right)\right\}, \quad (15)$$

$$C_{3D}^B(\rho) = \mathbb{E}\left\{\log_2 \det\left(\mathbf{I} + \frac{\text{SNR}}{\beta M}\left(\rho^2 \mathbf{G}^H \mathbf{R}_{Rx}^{2D}\mathbf{G}\mathbf{R}_{Tx}^{2D}\right.\right.\right.$$

$$\left.\left.\left. +\rho(1-\rho)\mathbf{R}_{mix} + (1-\rho)^2 \mathbf{R}_{i.i.d}\right)\right)\right\}, \quad 0 \le \rho \le 1, \quad (16)$$

where $\mathbf{R}_{mix} = \mathbf{G}^H \mathbf{I}_{Rx}\mathbf{G}\mathbf{R}_{Tx}^{2D} + \mathbf{G}^H \mathbf{R}_{Rx}^{2D}\mathbf{G}\mathbf{I}_{Tx}$ is a mixed component when $\mathbf{R}_{Rx} = \mathbf{I}_{Rx}$ or $\mathbf{R}_{Tx} = \mathbf{I}_{Tx}$, $\mathbf{R}_{i.i.d} = \mathbf{G}^H \mathbf{I}_{Rx}\mathbf{G}\mathbf{I}_{Tx}$ denotes the i.i.d correlation component when both $\mathbf{R}_{Rx} = \mathbf{I}_{Rx}$ and $\mathbf{R}_{Tx} = \mathbf{I}_{Tx}$. Here, $\mathbf{I}_{Tx}$ and $\mathbf{I}_{Rx}$ denote the unit matrix in a dimension of $M \times M$ and $Q \times Q$, respectively.

Proof: See Appendix IV-B

Lemma 3: Picking different values of ρ in (16), we can obtain the loose and tight bounds for 3D channel capacity:

(1) loose bound: $C_{2D} = C_{3D}^B(1) \le C_{3D} \le C_{3D}^B(0) \triangleq C_{i.i.d}$.

(2) tight bound: $C_{3D}^{low} \triangleq C_{3D}^B(\rho_0) \le C_{3D} \le C_{3D}^B(\rho_1) \triangleq C_{3D}^{up}$, with $\rho_0 = 1 - 2\pi^2 \, d_{z,0}^2 \varepsilon^2/3$, $\rho_1 = 1 - 2\pi^2 \, d_{z,1}^2 \varepsilon^2/3$, where ε denotes the EAS, $d_{z,0}$ and $d_{z,1}$ denote the minimum and maximum vertical spacing between antenna pairs, respectively.

Proof: See Appendix IV-C

As we can see, $C_{2D} \le C_{3D}^{low} \le C_{3D} \le C_{3D}^{up} \le C_{i.i.d}$. In Fig. 4, we examine the capacity bounds in Lemma 3 for a 32×8 MIMO system (4×4 cross-polarized pairs at the Tx, 2×2 cross-polarized pairs at the Rx) with $d_y = 0.5\lambda$, $d_z = 0.5\lambda$, $d_{z,0} = d_z$, $d_{z,1} = 3 \, d_z$ under different EASs. A large capacity gap between C_{3D} and C_{2D} can be observed (38.4% at SNR=25 dB, EAS=10°) and larger EAS values will expand the gap. The derived tight bounds fit well with C_{3D} for both EAS=10° and 20°. By increasing the EAS, C_{3D} tends to $C_{i.i.d}$.

IV. CONCLUSION

We investigate the superiority of the 3D channel over its conventional 2D counterpart in terms of SC and channel capacity. Given the cross-polarized URA and the standards based radiation patterns, an approximate closed-form expression for 3D SC has been derived with high approximation accuracy. By using the elevation domain (VAS and EAS), the 3D channel has a much lower SC than the 2D counterpart, and a higher channel capacity is expected with capacity bounds being derived in Lemma 3. These analyses highlight the significance of the elevation domain and indicate a promising future for 3D channel utilization.

APPENDIX

A. Proof of Lemma 1

Assuming a uniform distribution for the azimuth angle, (1) can be rewritten as

$$R_{mm'}^{3D} = R_{mm'}^{3D,\text{Num}} / R_{mm'}^{3D,\text{Den}}, \quad (17)$$

where $R_{mm'}^{3D,\text{Num}}$ is given in (18), at the top of the next page. Then, (19) is obtained via the Fourier series expansion, $A_H(\Phi) = \sum_{n=0}^N a_n \cos(n\Phi)$, and the transform $d_x \sin\theta \cos\phi + d_y \sin\theta \sin\phi = d_{xy} \sin\theta \cos(\phi - \Delta)$. The decomposition $\cos(n\Phi) = \cos(n(\Phi - \Delta))\cos(n\Delta) + \sin(n(\Phi - \Delta))\sin(n\Delta)$ and integration of the azimuth angle over $[-\pi, \pi]$ in (20) gives (21). Using (9), the approximation $A_V(\theta) f_1(\theta) \approx \sin(\theta)^{2L}$ and the expansion of $\sin(\theta)^{2L}$ [12, eq. (1.320.1)] where

$$\sin(\theta)^{2L} = \sum_{l=0}^L k_l \cos(2l\theta), \quad (22)$$

with k_l defined in (12), we get (24) (top of next page). Further simplifications of (23) leads to (24), then (25) based on [12, eq. (6.681.9)]. Meanwhile, $R_{mm'}^{3D,\text{Den}}$ in (17) is

$$R_{mm'}^{3D,\text{Den}} = \int_0^\pi A_V(\theta) f(\theta) d\theta \int_{-\pi}^\pi 10^{-1.2\left(\frac{\phi}{\phi_{3dB}}\right)^2} \frac{1}{2\pi} d\phi$$

$$= \int_0^\pi c_\kappa A_V(\theta) f_1(\theta) d\theta \int_{-\pi}^\pi \sum_{n=0}^N a_n \cos(n\phi) \frac{1}{2\pi} d\phi$$

$$= a_0 c_\kappa \int_0^\pi A_V(\theta) f_1(\theta) d\theta \approx a_0 c_\kappa \int_0^\pi \sin(\theta)^{2L} d\theta$$

$$= a_0 c_\kappa \int_0^\pi \sum_{l=0}^L \kappa_l \cos(2l\theta) d\theta = \pi a_0 k_0 c_\kappa. \quad (26)$$

Substituting (25) and (26) into (17) gives the desired result of (6) in Lemma 1.

B. Proof of Lemma 2

Substituting (13) into (14), we have $C_{2D} =$

$$\mathbb{E}\left\{\log_2 \det\left(\mathbf{I} + \frac{\text{SNR}}{\beta M}(\mathbf{R}_{Tx}^{2D})^{\frac{1}{2},H}\mathbf{G}^H(\mathbf{R}_{Rx}^{2D})^{\frac{1}{2},H}(\mathbf{R}_{Rx}^{2D})^{\frac{1}{2}}\mathbf{G}(\mathbf{R}_{Tx}^{2D})^{\frac{1}{2}}\right)\right\}$$

$$= \mathbb{E}\left\{\log_2 \det\left(\mathbf{I} + \frac{\text{SNR}}{\beta M}(\mathbf{R}_{Tx}^{2D})^{\frac{1}{2},H}\mathbf{G}^H \mathbf{R}_{Rx}^{2D}\mathbf{G}(\mathbf{R}_{Tx}^{2D})^{\frac{1}{2}}\right)\right\}, \quad (27)$$

simplifications of (27) give that [13, Corollary 18.1.2] C_{2D}

$$= \mathbb{E}\left\{\log_2 \det\left(\mathbf{I} + \frac{\text{SNR}}{\beta M}\mathbf{G}^H \mathbf{R}_{Rx}^{2D}\mathbf{G}(\mathbf{R}_{Tx}^{2D})^{\frac{1}{2}}(\mathbf{R}_{Tx}^{2D})^{\frac{1}{2},H}\right)\right\} \quad (28)$$

which gives the desired result in (15). Similarly, we have

$$C_{3D} = \mathbb{E}\left\{\log_2 \det\left(\mathbf{I} + \frac{\text{SNR}}{\beta M}\mathbf{G}^H \mathbf{R}_{Rx}^{3D}\mathbf{G}\mathbf{R}_{Tx}^{3D}\right)\right\}. \quad (29)$$

From [5, eq. (29)], 3D SC can be further decomposed as

$$\mathbf{R}_{Rx}^{3D} \approx \mathbf{R}_{Rx}^{2D} \odot \mathbf{R}_{Rx}^{el}, \quad \mathbf{R}_{Tx}^{3D} \approx \mathbf{R}_{Tx}^{2D} \odot \mathbf{R}_{Tx}^{el}, \quad (30)$$

where $\mathbf{R}_{Rx}^{el}$ and $\mathbf{R}_{Tx}^{el}$ denote the elevation SC matrix at the Rx and Tx, respectively.

As lower SC between antenna elements lead to higher capacity, SC matrix with all non-diagonal values being the maximum/minimum value lead to the lower/upper bound on

$$R_{mm'}^{\text{3D,Num}} = \int_\theta \left(\int_{-\pi}^{\pi} A_{\text{H}}(\phi) e^{-j2\pi(d_x \sin\theta\cos\phi + d_y \sin\theta\sin\phi)} \frac{1}{2\pi} d\phi \right) A_{\text{V}}(\theta) f(\theta) e^{-j2\pi d_z \cos\theta} d\theta \tag{18}$$

$$= \int_\theta \left(\int_{-\pi}^{\pi} \sum_{n=0}^{N} a_n \cos(n\phi) e^{-j2\pi d_{xy}\sin\theta\cos(\phi-\Delta)} \frac{1}{2\pi} d\phi \right) c_\kappa A_{\text{V}}(\theta) f_1(\theta) e^{-j2\pi d_z \cos\theta} d\theta \tag{19}$$

$$= \sum_{n=0}^{N} a_n c_\kappa \int_\theta \left(\int_{-\pi}^{\pi} \cos(n(\phi-\Delta)) \cos(n\Delta) e^{-j2\pi d_{xy}\sin\theta\cos(\phi-\Delta)} \frac{1}{2\pi} d\phi + 0 \right) A_{\text{V}}(\theta) f_1(\theta) e^{-j2\pi d_z \cos\theta} d\theta \tag{20}$$

$$= \sum_{n=0}^{N} a_n (-j)^n \cos(n\Delta) c_\kappa \int_0^{\pi} J_n(2\pi d_{xy}\sin\theta) A_{\text{V}}(\theta) f_1(\theta) e^{-j2\pi d_z \cos\theta} d\theta \tag{21}$$

$$R_{mm'}^{\text{3D,Num}} \approx \sum_{n=0}^{N} a_n (-j)^n \cos(n\Delta) c_\kappa \int_0^{\pi} J_n(2\pi d_{xy}\sin\theta) \sum_{l=0}^{L} k_l \cos(2l\theta) \left(J_0(-2\pi dz) + 2 \sum_{r=1}^{R} j^r J_r(-2\pi d_z) \cos(r\theta) \right) d\theta \tag{23}$$

$$= \sum_{n=0}^{N} a_n (-j)^n \cos(n\Delta) c_\kappa \sum_{l=0}^{L} k_l \left[J_0(-2\pi dz) \int_0^{\pi} J_n(2\pi d_{xy}\sin\theta) \cos(2l\theta) d\theta + \sum_{r=1}^{R} j^r J_r(-2\pi d_z) \right.$$
$$\left. \times \int_0^{\pi} J_n(2\pi d_{xy}\sin\theta) \left(\cos((r-2l)\theta) + \cos((r+2l)\theta) \right) \right] d\theta \tag{24}$$

$$= \sum_{n=0}^{N} a_n (-j)^n \cos(n\Delta) c_\kappa \left\{ \sum_{l=0}^{L} k_l \pi \left[J_0(-2\pi d_z) J_{\frac{n}{2}-l}(\pi d_{xy}) J_{\frac{n}{2}+l}(\pi d_{xy}) + \sum_{r=1}^{R} j^r J_r(-2\pi d_z) \right. \right.$$
$$\left. \left. \times \left(\cos(N_{1r}\pi) J_{\frac{n}{2}-N_{1r}}(\pi d_{xy}) J_{\frac{n}{2}+N_{1r}}(\pi d_{xy}) + \cos(N_{2r}\pi) J_{\frac{n}{2}-N_{2r}}(\pi d_{xy}) J_{\frac{n}{2}+N_{2r}}(\pi d_{xy}) \right) \right] \right\} \tag{25}$$

---

channel capacity, e.g., defining the bounding elevation SC matrix $\mathbf{R}_{\text{Rx}}^{\text{el,B}}$ and $\mathbf{R}_{\text{Tx}}^{\text{el,B}}$ which satisfy

$$[\mathbf{R}_{\text{Rx}}^{\text{el,B}}]_{ij} = \rho, \ [\mathbf{R}_{\text{Tx}}^{\text{el,B}}]_{pq} = \rho, \ (i \neq j, p \neq q), \tag{31}$$

where $\rho = max$ (or min)$\{|[\mathbf{R}_{\text{Rx}}^{\text{el}}]_{ij}|, |[\mathbf{R}_{\text{Tx}}^{\text{el}}]_{pq}|, (i \neq j, p \neq q)\}$. Then, rewrite $\mathbf{R}_{\text{Rx}}^{\text{el,B}}$ and $\mathbf{R}_{\text{Tx}}^{\text{el,B}}$ as

$$\mathbf{R}_{\text{Rx}}^{\text{el,B}} = \rho \mathbf{E}_{\text{Rx}} + (1-\rho)\mathbf{I}_{\text{Rx}}, \quad \mathbf{R}_{\text{Tx}}^{\text{el,B}} = \rho \mathbf{E}_{\text{Tx}} + (1-\rho)\mathbf{I}_{\text{Tx}}, \tag{32}$$

where $\mathbf{E}_{\text{Rx}}$ and $\mathbf{E}_{\text{Tx}}$ denote the matrix with all elements being 1 in a dimension of $Q \times Q$ and $M \times M$, respectively. Thirdly, substituting (32) into (30), the bounding SC matrix $\mathbf{R}_{\text{Rx}}^{\text{3D,B}}$ and $\mathbf{R}_{\text{Tx}}^{\text{3D,B}}$ are calculated as

$$\mathbf{R}_{\text{Rx}}^{\text{3D,B}} = \mathbf{R}_{\text{Rx}}^{\text{2D}} \odot \mathbf{R}_{\text{Rx}}^{\text{el,B}} = \rho \mathbf{R}_{\text{Rx}}^{\text{2D}} + (1-\rho)\mathbf{I}_{\text{Rx}}, \tag{33}$$
$$\mathbf{R}_{\text{Tx}}^{\text{3D,B}} = \mathbf{R}_{\text{Tx}}^{\text{2D}} \odot \mathbf{R}_{\text{Tx}}^{\text{el,B}} = \rho \mathbf{R}_{\text{Tx}}^{\text{2D}} + (1-\rho)\mathbf{I}_{\text{Tx}}. \tag{34}$$

Finally, substituting (33) and (34) into (29), further simplifications will give the desired bounding capacity $C_{\text{3D}}^B(\rho)$ in (16).

C. Proof of Lemma 3

A larger non-diagonal value of SC matrix, ρ in (31), will lead to a smaller channel capacity. When $\rho = 1$ and 0, we obtain the loose lower bound C_{2D} and upper bound $C_{\text{i.i.d}}$, respectively. Under small EAS case, $[\mathbf{R}_{\text{Rx}}^{\text{el}}]_{ij} = 1 - 2\pi^2 d_{z,ij}^2 \varepsilon^2/3$, $[\mathbf{R}_{\text{Tx}}^{\text{el}}]_{pq} = 1 - 2\pi^2 d_{z,pq}^2 \varepsilon^2/3$ (from [5, Lemma 1]), where $d_{z,ij}, d_{z,pq}$ denote the vertical spacing between the ith and j^{th} Rx element, the pth and q^{th} Tx element, respectively. Thus the maximum and minimum value of ρ in (31), ρ_0 and ρ_1, can be obtained by picking the minimum and maximum vertical spacing from $\{d_{z,ij}, d_{z,pq}, (i \neq j, p \neq q)\}$, respectively. When $\rho = \rho_0$, we get the tight lower bound C_{3D}^{low}. When $\rho = \rho_1$, we get the tight upper bound C_{3D}^{up}.

REFERENCES

[1] *Framework and Overall Objectives of the Future Development of IMT for 2020 and Beyond*, ITU-R, San Diego, CA, USA, Jun. 2015.

[2] J. Zhang *et al.*, "3-D MIMO: How much does it meet our expectations observed from channel measurements?" *IEEE J. Sel. Areas Commun.*, vol. 35, no. 8, pp. 1887–1903, Aug. 2017.

[3] A. Kammoun *et al.*, "Preliminary results on 3D channel modeling: From theory to standardization," *IEEE J. Sel. Areas Commun.*, vol. 32, no. 6, pp. 1219–1229, Jun. 2014.

[4] Y. Yu *et al.*, "3D vs. 2D channel capacity of outdoor to indoor scenarios derived from measurements in China and New Zealand," in *Proc. 24th Eur. Signal Process. Conf. (EUSIPCO)*, Aug. 2016, pp. 1980–1984.

[5] Y. Yu *et al.*, "3D vs. 2D channel models: Spatial correlation and channel capacity comparison and analysis," in *Proc. IEEE Int. Conf. Commun. (ICC)*, May 2017, pp. 1–7.

[6] S. K. Yong and J. S. Thompson, "Three-dimensional spatial fading correlation models for compact MIMO receivers," *IEEE Trans. Wireless Commun.*, vol. 4, no. 6, pp. 2856–2869, Nov. 2005.

[7] K. Rosengren and P. S. Kildal, "Radiation efficiency, correlation, diversity gain and capacity of a six-monopole antenna array for a MIMO system: Theory, simulation and measurement in reverberation chamber," *IEE Proc.-Microw., Antennas Propag.*, vol. 152, no. 1, pp. 7–16, Feb. 2005.

[8] Q.-U.-A. Nadeem *et al.*, "A generalized spatial correlation model for 3D MIMO channels based on the Fourier coefficients of power spectrums," *IEEE Trans. Signal Process.*, vol. 63, no. 14, pp. 3671–3686, Jul. 2015.

[9] *Study on 3D Channel Model for LTE (Release 12)*, document 3GPP TR 36.873 V.2, 2014.

[10] D. Ying *et al.*, "Kronecker product correlation model and limited feedback codebook design in a 3D channel model," in *Proc. IEEE Int. Conf. Commun. (ICC)*, Jun. 2014, pp. 5865–5870.

[11] D. P. Palomar *et al.*, "Capacity results of spatially correlated frequency-selective MIMO channels in UMTS," in *Proc. IEEE VTS 54th Veh. Technol. Conf. (VTC Fall)*, vol. 2. Oct. 2001, pp. 553–557.

[12] I. S. Gradshteĭn and I. M. Ryžik, *Table of Integrals, Series, and Products*, 7th ed. San Francisco, CA, USA: Academic, 2014.

[13] D. A. Harville, *Matrix Algebra From a Statistician's Perspective*, vol. 1. New York, NY, USA: Springer, 1997.